Remote sensing technology for rapid extraction of burned areas and ecosystem environmental assessment

Shiqi Zhang[1], Maoyang Bai[1], Xiao Wang[2], Xuefeng Peng[3], Ailin Chen[4,5] and Peihao Peng[1,3]

[1] College of Earth Sciences, Chengdu University of Technology, Chengdu, China
[2] School of Architecture and Civil Engineering, Chengdu University, Chengdu, China
[3] College of Tourism and Urban-Rural Planning, Chengdu University of Technology, Chengdu, China
[4] Sichuan Earthquake Agency, Chengdu, China
[5] Chengdu lnstitute of Tibetan Plateau Earthquake Research, China Earthquake Administration, Chengdu, China

Corresponding authors
Maoyang Bai,
baimaoyang@outlook.com
Peihao Peng, peihaop@163.com

ABSTRACT

Forest fires are one of the significant disturbances in forest ecosystems. It is essential to extract burned areas rapidly and accurately to formulate forest restoration strategies and plan restoration plans. In this work, we constructed decision trees and used a combination of differential normalized burn ratio (dNBR) index and OTSU threshold method to extract the heavily and mildly burned areas. The applicability of this method was evaluated with three fires in Muli County, Sichuan, China, and we concluded that the extraction accuracy of this method could reach 97.69% and 96.37% for small area forest fires, while the extraction accuracy was lower for large area fires, only 89.32%. In addition, the remote sensing environment index (RSEI) was used to evaluate the ecological environment changes. It analyzed the change of the RSEI level through the transition matrix, and all three fires showed that the changes in RSEI were stronger for heavily burned areas than for mildly burned areas, after the forest fire the ecological environment (RSEI) was reduced from good to moderate. These results realized the quantitative evaluation and dynamic evaluation of the ecological environment condition, providing an essential basis for the restoration, decision making and management of the affected forests.

INTRODUCTION

Forests, the terrestrial ecosystems' mainstay, are the foundation of human survival and development (*Mitchard, 2018*; *Gao et al., 2020*). Forest fires are fast-spreading, sudden and difficult to control. They cause massive forest damage and severely affect the composition of ecosystems, leading to a dramatic reduction in biomass and drastic changes in the landscape and the global carbon cycle (*Xaud, da Martins & Dos Santos, 2013*; *De Faria et al., 2017*; *Liu, Ballantyne & Cooper, 2019*; *Zhao et al., 2021b, 2021a*). In recent years, global warming and frequent human production activities have increased forest fires

worldwide (*Hall et al., 2016*; *Forkel et al., 2019*; *Vargas-Cuentas & Roman-Gonzalez, 2021*). The forest fire prevention industry is facing a more complex situation, so new requirements and challenges for the restoration work after the disaster (*Andela et al., 2017*). It is critical to rapidly and accurately extract the extent of burned areas in forests, enabling the timely development of forest restoration strategies and plans (*Pezzatti et al., 2020*; *Kim, Hwang & Choi, 2021*). Traditionally, the burned area of forest fires is delineated by manual field surveys, but this method is generally labor-intensive and costly because of the complex topography of the southwestern forest area (*Mitri & Gitas, 2008*; *Gitas et al., 2012*). Satellite remote sensing has significant advantages in extracting the burned areas and assessing ecological changes in the forest fires, with its short imaging period and wide monitoring range. The theory is that vegetation reduces chlorophyll content after fire burning, and the reduction of chlorophyll causes wavelength changes in the visible, red-edge and near-infrared (NIR) wavelengths (*Mueller et al., 2017*; *Ba et al., 2019*; *Reddy et al., 2019*; *Chuvieco et al., 2020*; *Laneve et al., 2020*; *Santana et al., 2020*; *Sudhakar et al., 2020*). The index threshold method is the most commonly used, which separates the burned area by analyzing the spectral reflectance curve of the burned area, selecting the appropriate waveband to establish the index, and choosing the appropriate threshold to separate the burned area. The Burned Area Index (BAI) (*Chuvieco, Martín & Palacios, 2010*), Normalized Burn Ratio (NBR) (*Cocke, Fulé & Crouse, 2005*), Mid-InfraRed Bispectral Index (MIRBI) (*Smith et al., 2007*) and other indices were derived successively. In addition, the Normalized Divergence Vegetation Index (NDVI), Soil-Adjusted Vegetation Index (SAVI), Global Environment Monitoring Index (GEMI), Enhanced Vegetation Index (EVI) and other remote sensing vegetation indices are also commonly used in burned areas mapping (*Sun et al., 2019*). It has been found that NBR can be used as an indicator of burn severity in forested areas (*Epting, Verbyla & Sorbel, 2005*). Several global burned areas products have been released in the past few years, mainly from remote sensing satellite sensors such as MODIS, MERIS, or VEGETA, which have a higher temporal resolution but a lower spatial resolution (>300 m) and cannot extract burned area more accurately (*Hall et al., 2016*; *Forkel et al., 2019*; *Santana et al., 2020*; *Valencia et al., 2020*; *Franquesa et al., 2022*). Sentinel-2 and Landsat data, which can provide more detailed high-resolution remote sensing images, also bring further accuracy improvement to the regional forest burned area extraction (*Roteta et al., 2021*). Traditional threshold determination is an artificially selected threshold, which may artificially bias the results (*Giri, Qiu & Zhang, 2017*; *Sekertekin, 2021*). The OTSU algorithm is a classical adaptive thresholding segmentation algorithm, and it uses the maximum inter-class variance adaptation to determine the optimal threshold to achieve the best segmentation effect. The OTSU algorithm is computationally simple and independent of image brightness and contrast, so it is widely used in automated extraction (*Otsu, 1996*; *Huang & Jin, 2020*; *Pan, Xi & Wang, 2020*; *Dutta, Talukdar & Bora, 2022*). Fire can cause forest damage to different degrees, generally divided into fire-traced areas (called mildly burned areas) and forest loss areas (called heavily burned areas) (*Rao, Wang & Huang, 2020*). Available burned area products do not break down the burned areas with different damage (*Santana et al., 2020*; *Valencia et al., 2020*). However, the length of restoration and subsequent management of

different damaged forests is different, so it is necessary to classify the burned areas. Decision Tree Learning (DTL) is a critical remote sensing extraction method in the process of statistics, data mining and machine learning, which divides samples through hierarchical progressive attribute judgments. The decision tree is widely used in remote sensing image classification extraction as an efficient yet simple machine learning method (*Yang et al., 2003*; *Zhou, Zhang & Zhang, 2016*; *Verma, Garg & Hari Prasad, 2017*; *Zhang et al., 2017*; *Ghatkar, Singh & Shanmugam, 2019*). There have been studies using the decision tree to build a combination of the burning index and OTSU thresholds to extract burned areas (*Tianchi, Fuqin & Yan, 2020*; *Li et al., 2021a*; *Tang et al., 2021*; *Tian et al., 2022*), which can achieve better accuracy results. There are also comparative studies on the extraction of the burned area from Sentinel-2 and Landsat 8 data sources, and they found that Sentinel generally performed as well or better than Landsat for four spectral indices of burn severity and that Sentinel's higher spatial resolution improves opportunities for examining finer-scale fire effects across ecosystems (*Mallinis, Mitsopoulos & Chrysafi, 2018*; *Zhang et al., 2019*; *Howe et al., 2022*). However, the extraction and evaluation of burned areas with different damage using Sentinel-2 are lacking, so assessing the method's applicability is necessary. The Google Earth engine (GEE) is a tool that can batch-process satellite image data. It can process large amounts of images quickly and in batches compared with traditional tools for processing images, and is one of the most popular remote sensing processing tools available. It is also starting to be used in burned area extraction (*Roteta et al., 2021*; *Seydi et al., 2021*). In this study, we evaluated the applicability of the dNBR and OTSU threshold methods based on the GEE platform for the extraction of heavy and mildly burned areas from three forest fires.

On the other hand, the ecological environment of burned areas changes significantly after the fire, such as soil, moisture, and biology. Firstly, the structure and quantity of plants and leaves are limited, with a corresponding decrease in chlorophyll and overall environmental moisture. The most apparent change is the increase in soil temperature, the magnitude of which is closely related to fire intensity, fire duration, and soil moisture content. These effects can be reflected by moisture, greenness, heat and dryness indicators: soil moisture and vegetation water content caused changes in wetness. Vegetation health status caused changes in greenness, soil temperature and ground cover caused changes in heat, soil temperature and land degradation caused dryness changes (*Attorre et al., 2015*; *Chia et al., 2016*; *Day et al., 2020*). There are some studies on the dynamic changes of vegetation in the study area before and after forest fires (*Zhou et al., 2019*), but less monitoring of ecological damage before and after the forest fires. Remote sensing technology has strong advantages for monitoring ecological changes. The remote sensing ecological index (RESI) is entirely based on remote sensing information technology, which reduces the subjectivity and difficulty of index extraction in practical applications and facilitates large-scale and continuous investigation and observation (*Xu, 2013*). It can be used to reflect the comprehensive status of regional ecological quality (*Jiang et al., 2021*; *Yuan et al., 2021*; *Lian et al., 2022*; *Wang & Li, 2022*). It couples four indicators that intuitively reflect the superiority or inferiority of ecological quality status, such as wetness,
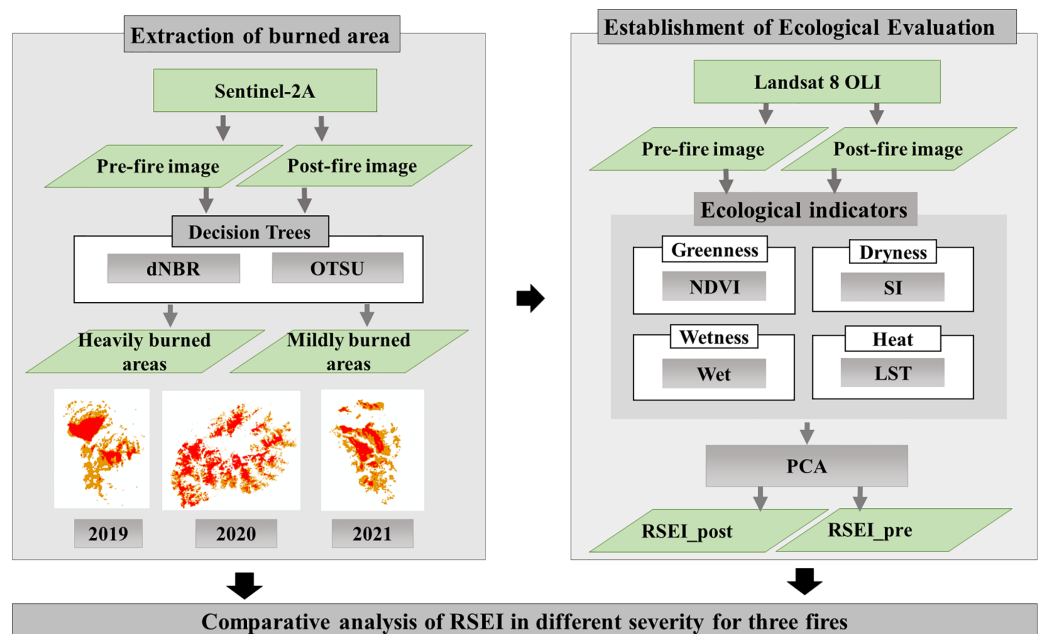
Figure 1 The workflow.

greenness, heat and dryness, characterized by humidity index, normalized vegetation index, surface temperature and dryness index, respectively.

Muli County is located in the Southwest Forest Region, one of the most frequent areas where forest fires occur in China. Muli County had forest fires for three consecutive years in 2019, 2020 and 2021. It has a complex landscape with high and low relief and rugged closed terrain. Once a fire occurs, the high mountain and steep slope environment accelerates the fire's spread and exacerbates the difficulty of extinguishing it. Therefore, Muli County is a high-risk area for forest fires and a key area of national fire risk (*Li et al., 2021b*). In this work, taking Muli County, where fires occurred for three consecutive years, as the study area, we used the dNBR index of sentinel-2 remote sensing images, combined with the OTSU thresholding method and decision tree to extract the heavily burned areas and mildly burned areas. In addition, we evaluated the ecological environment changes by using RSEI and analyzing them to achieve the quantitative evaluation of ecological environment status and dynamic evaluation.

MATERIALS AND METHODS

This work is divided into three main sections. The materials and methods are shown in the following Figure (Fig. 1).

Extraction of the burned area

This work used the GEE cloud platform to rapidly extract the burned area caused by three major fires in Muli County in 2019, 2020, and 2021, and the extraction process is as follows: Firstly, Sentinel-2A images were acquired one month after the fire was extinguished, and the median was synthesized as the post-fire image; Considering the phenological cycle of the vegetation in the study area, the Sentinel-2A images were also

Table 1 Time of the images acquisition.

Time of fire	Post-fire image	Pre-fire image
March 30, 2019	April 10–May 10, 2019	April 10–May 10, 2018
March 28, 2020	April 7–May 7, 2020	April 7–May 7, 2019
April 5, 2021	April 9, 2021–May 9, 2021	April 9, 2021–May 9, 2020

acquired one year before that period, and the median was synthesized as the pre-fire image, and the specific image acquisition time is shown in the following Table 1.

Secondly, we constructed a decision tree to extract the burned area; we used the NIR and SWIR bands to calculate the NBR index in pre-fire images and the NBR index in post-fire images, and calculated the dNBR, then the OTSU algorithm was used to calculate the dNBR threshold1 to extract heavily burned area, and used this result to mask the heavily burned area and keep the other parts. Finally, the OTSU algorithm was used again to classify and extract the mildly burned areas.

Establishment of ecological evaluation

The remote sensing ecological index (RSEI) be used to evaluate the ecological and environmental of the burned area. It integrates moisture, greenness, heat and dryness information using principal component analysis.

Comparative analysis of RSEI in different severity for three fires

We resample the extracted burning area to 30 m, with the same spatial resolution of RSEI, and compare the variation of RSEI for different severity for three fires.

Study area

Muli County is located on the southeastern edge of the Qinghai-Tibet Plateau (longitude 100°03′–101°41′ east, latitude 27°40′–29°10′ north), at the boundary between the Qinghai-Tibet Plateau and the Yunnan-Guizhou Plateau. Its main landform features are mountains, canyons and mountain plains. The terrain is complex, and the altitude difference a are enormous. It belongs to a typical alpine and canyon area. Muli County has a subtropical monsoon climate, with rainy summers and less rain in winter. Muli is rich in forest resources, with a forest coverage rate of 67.3%, including *Picea asperata*, *Quercus semicarpifolia*, *Pinus densata*, *etc.*, and more than 10 kinds of national first and second-class protected tree species. The volume of standing trees is 117 million m^2, accounting for 10% of Sichuan Province and 1% of the whole country (*Liu, 2014*), and the vegetation is vertically distributed.

The annual average temperature is about 14.0 °C, the temperature difference between day and night is significant, and solar radiation is powerful. The four seasons are not pronounced, and the dry and wet seasons are distinct. The dry season is from December to March of the following year., the climate is dry, with little precipitation, long sunshine hours, and uneven spatial and temporal distribution of precipitation, often suffering from natural disasters such as droughts, debris flows and floods (*Li et al., 2021d*, *2021c*). The wet season is from June to September, the precipitation is concentrated, the rainfall is abundant, the daily temperature difference is slight, and the climate is suitable. The forest
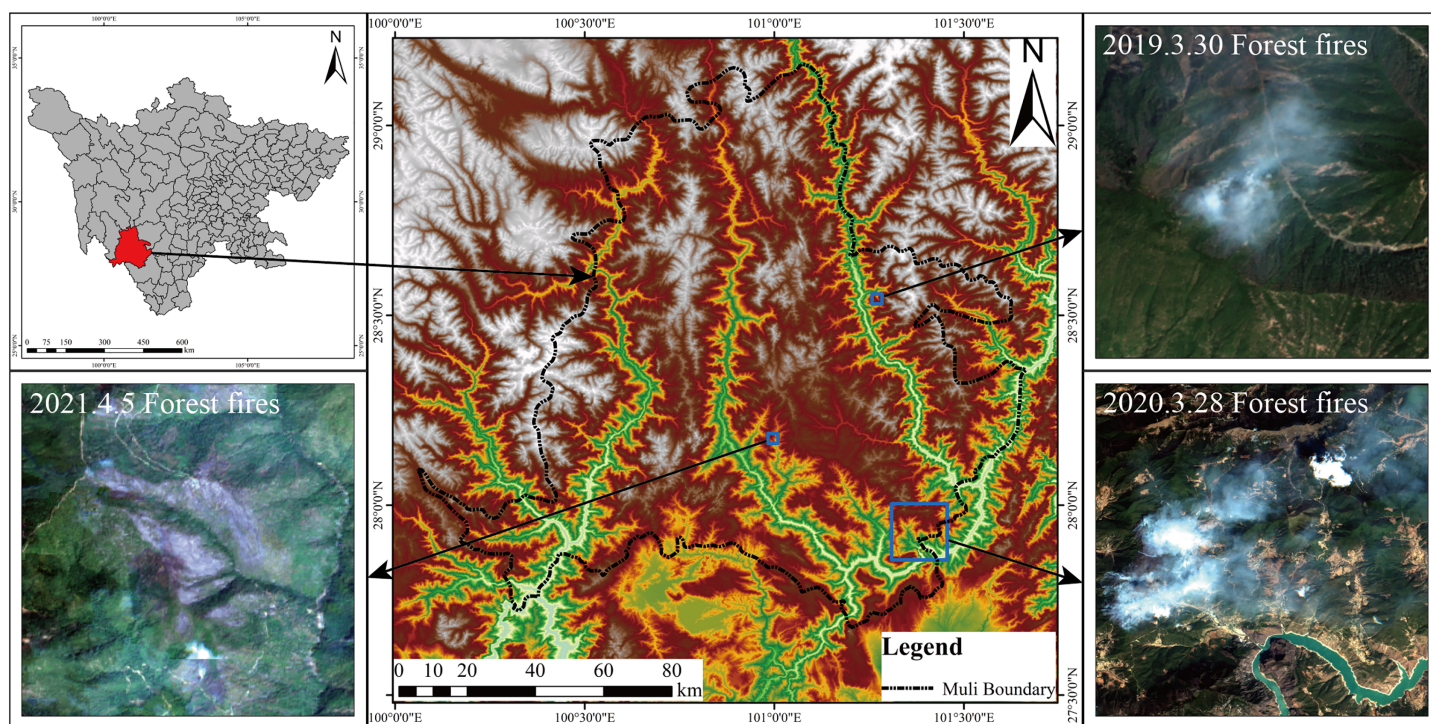
Figure 2 Location of the study area (forest fires images are from Sentinel-2).

in the study area is widely distributed, the terrain is complex and changeable, and the forest fire prevention situation is complicated. Forest fires have occurred in the region for three consecutive years, causing massive casualties, economic losses and loss of forest resources. The fire areas are shown in Fig. 2:

Data

Satellite images

The remote sensing images used in this work are sentinel-2 and Landsat 8 OLI from the Google Earth Engine Cloud Platform (https://code.earthengine.google.com/). The Sentinel-2 L2A dataset, which ESA had pre-processed for radiometric calibration, atmospheric correction, *etc*., reflects the reflectance information at the surface; this dataset is used to extract the burned areas in the study area. The Landsat 8 Level 2 Collection 2 Tier 1 is a reflectance product created by the Land Surface Reflectance Code (LaSRC) and processed by a single-pass algorithm, including radiometric and geometric correction datasets. Both datasets can be used without subsequent processing. The data information is shown in Table 2:

Reference data

The reference data are the fire survey data of the Sichuan Forestry Survey and Design Institute. It was vector data that was visually interpreted from sentinel-2 remote sensing images and corrected using field verification. The reference data mainly includes the forest

Table 2 Data information.

Datasets	Temporal resolution	Spatial resolution
Sentinel-2 L2A	5 days	10 m
Landsat 8 Level 2 Collection 2 Tier 1	16 days	30 m

Table 3 The statistical table of fire area survey.

Time of fire	Burned area (hm^2)		
	Heavily burned area	mildly burned area	Total burned area
March 30, 2019	43.90	74.19	118.09
March 28, 2020	8,856.05	8,547.84	17,403.89
April 5, 2021	66.12	150.26	216.38

loss area (heavily burned area), the forest where fire passed area (forest loss is not apparent, mildly burned area), and various survey data details are shown in Table 3.

dNBR computation

The NBR (Normalized Burn Ratio) is a remote sensing index obtained by replacing the red band in the NDVI (Normalized Difference Vegetation Index) equation with the SWIR band. Since the reflectance change in the NIR in the burned areas is more significant than that in the SWIR compared with the non-burned areas, it can be used as an essential indicator factor to extract burned areas. The NBR values range from 1 to −1 and negatively correlate with forest fire intensity. However, the NBR index has some advantages in the extraction of burned areas, but using the mono-temporal NBR is still affected by low reflectivity areas such as water bodies, which is prone to significant errors. The dNBR (delta Normalized Bun Ratio) (*Chen, Loboda & Hall, 2020*) utilized a multi-temporal that is the difference of NBR index in the post-fire images and pre-fire images, and it can effectively reduce the influence of factors such as clouds and aerosols compared with the NBR index.

Moreover, it can be seen that the NBR reflectance of burned areas showed an increase after the occurrence of forest fires. In contrast, the SWIR reflectance of burned areas is extremely sensitive to water bodies, and the vegetation humidity in the forest decreases after burning, so the higher the intensity of the forest fire, the more significant the decrease in humidity within the forest and the decrease in humidity then leads to the decrease the SWIR reflectance. Finally, the NBR index shows a decrease. Therefore, the dNBR index of the burned area images is significantly higher than the low reflectance areas such as water bodies. In summary, the dNBR index of multi-temporal can be used to distinguish the burned areas. The NBR's and the dNBR's mathematical formulas are as Eqs. (1) and (2):

$$NBR = \frac{\rho_{nir} - \rho_{swir}}{\rho_{nir} + \rho_{swir}} \quad (1)$$

$$dNBR = NBR_{pre} - NBR_{post} \quad (2)$$

where ρ_{nir} represents the NIR band reflectance of sentinel-2 (Band 8); ρ_{swir} represents the SWIR band reflectance of sentinel-2 (Band 11); NBR_{pre} represents the pre-fire NBR index; NBR_{post} represents the post-fire NBR index.

OTSU thresholding for image segmentation

Threshold segmentation is one of the most commonly used image segmentation methods; it is simple and effective. Moreover, scholars have made researched the methods of automatically obtaining thresholds in image segmentation work. The OTSU algorithm, also known as the maximum interclass variance method, is an automatic algorithm for the global binarization of clustered images proposed by Japanese scholar Zhenyuki Otsu in 1979 (*Otsu, 1979*). It can obtain more ideal segmentation results, has the characteristics of high segmentation efficiency and broad application scenarios, the results are stable, and the segmentation quality can be guaranteed, so it has been widely used (*Fan et al., 2016*). It works as a discrete simulation of the one-dimensional Fisher discriminant. In computer vision and image processing work, this algorithm assumes that an image contains only two classes of pixels (background pixels and target pixels) after bimodal histogram processing and then minimizes their intra-class variance and maximizes inter-class variance by calculating the best threshold that can distinguish between the two classes of pixels.

The OTSU algorithm is computed as follows: Assuming that an image has several pixels, the probability of occurrence in each gray-level pixel P_i is Eq. (3):

$$P_i = {}^{n_i}\!/\!_N, (i = 0, 1, 2, 3 \ldots L-1), \sum_{i=0}^{L-1} P_i = 1 \quad (3)$$

where the grayscale i takes a range $[0, L-1]$, the number of pixels in the grayscale i level is n_i. The image was divided into background pixels C_0 and target pixels C_1 using thresholding, C_0 consisting of pixels with grayscale values $[0, k]$ and C_1 pixels with grayscale values $[t+1, L-1]$. Then, the probability of occurrence of each gray μ_t is Eq. (4):

$$\mu_t = \sum_{i=0}^{L-1} iP_i \quad (4)$$

The occurrence probability of C_0 and C_1 pixels are Eqs. (5) and (6):

$$\omega_0 = \sum_{i=0}^{L-1} P_i \quad (5)$$

$$\omega_1 = \sum_{i=t+1}^{L-1} P_i = 1 - \omega_0 \quad (6)$$

The average gray μ_0 and μ_i are Eqs. (7)–(9):
$$\mu_0 = \sum_{i=0}^{t} iP_i \Big/ \omega_0 \tag{7}$$

$$\mu_1 = \sum_{i=t+1}^{L-1} iP_i \Big/ \omega_1 \tag{8}$$

$$\mu_t = \omega_0 \mu_0 + \omega_1 \mu_1 \tag{9}$$

The interclass variance δ_t^2 is Eq. (10):

$$\delta_t^2 = \omega_0(\mu_0 - \mu_t)^2 + \omega_1(\mu_1 - \mu_t)^2 = \omega_0 \omega_1(\mu_0 - \mu_1)^2 \tag{10}$$

The optimal threshold to distinguish between the two classes of pixels is the one that takes the value in the interval when the maximum value is reached.

After a forest fire, there is a sharp increase in the maximum interclass variance within a reasonable image element window, and the OTSU algorithm was applied to extract the dNBR threshold automatically. It can be used as an essential parameter in active fire detection.

Building decision trees

Decision tree learning is an essential method in the field of statistics, data mining and machine learning, mainly used as a prediction model to analyze test and target variables in a round-robin manner and finally to predict the category of the samples. The training process is to obtain rules for classification by summarizing expert experience, simple statistical analysis of mathematical models, induction, *etc*. A training set is divided into several subsets, and the recursion is repeated in the resulting subsets. This top-down decision tree induction method is one of the greedy algorithms and is one of the most commonly used training methods, which can be applied in predicting continuous variables and remote sensing classification.

In this work, we constructed a decision tree classification model with the dNBR based on the sensitive feature analysis of burned areas. First, we divided burned areas into the mildly burned areas (fire traced area) and the heavily burned area (forest loss area) and calculated the first dNBR threshold based on OTSU, which was used to distinguish the heavily burned area (forest loss area). Then a second dNBR threshold is calculated in the rest area based on OTSU, which is used to distinguish between the mildly burned areas (fire traced area) as well as the rest area, and the decision tree classification model is shown in Fig. 3.

Accuracy verification

The accuracy verification of burned areas identification used the following calculation formula (Eq. (11)):

$$P = (1) - \left| \frac{a - b}{b} \right| \times 100\% \tag{11}$$
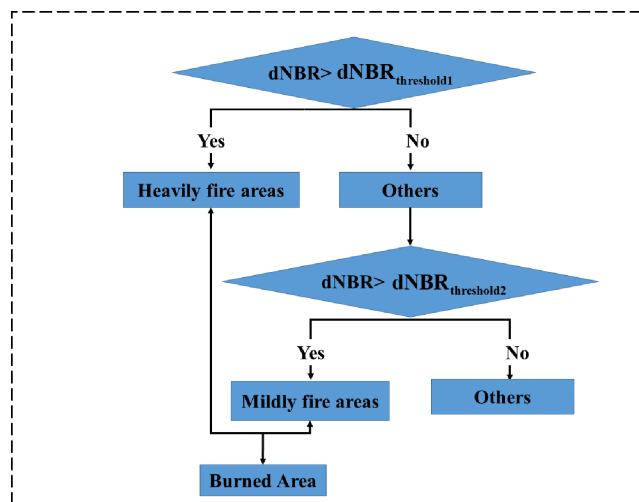
Figure 3 Decision tree classification model.

P represents the accuracy of the method, *a* represents the number of image elements of the identified burning area, and *b* represents the number of image elements visually interpreted after the field survey respectively.

To better verify the experimental results, we used the kappa coefficient to verify the accuracy. Its equation is as follows.

$$\text{Kappa} = \frac{P_o - P_e}{1 - P_e} \tag{12}$$

where P_o is the sum of the diagonals of the confusion matrix divided by the total number of samples, and P_e is the sum of the "product of actual and predicted numbers" for each of the categories, divided by the "square of the total number of samples".

Construction of a comprehensive ecological index

Therefore, the remote sensing ecological index (RSEI) is rapid monitoring and evaluation of the ecological method based on natural factors, which integrates moisture, greenness, heat and dryness information and can also be used to evaluate the ecological and environment of the burned area.

Greenness

In this work, the normalized vegetation index (NDVI) was selected to characterize the greenness of the study area, which can reflect the plant biomass, leaf area index and vegetation cover in the region, calculated as Eq. (13):

$$NDVI = \frac{\rho_{nir} - \rho_{red}}{\rho_{nir} + \rho_{red}} \tag{13}$$

where, ρ_{nir} and ρ_{red} represent the reflectance of Landsat images in the NIR and red bands, respectively.

Wetness

The wetness index is characterized based on the moisture component obtained from the tassel cap transformation, and the wetness can reflect the surface water body conditions, especially the moisture of the soil and the calculation method for wetness extraction based on Landsat8/OLI data is shown in Eq. (13) (*Baig et al., 2014*). Before extraction, the water bodies were masked using the Modified Normalized Difference Water Index (MNDWI) (*Sun, Wu & Tan, 2012*), so the wetness reflects the actual land surface moisture conditions.

$$Wet = 0.1511b_2 + 0.1973b_3 + 0.3283b_4 + 0.3407b_5 - 0.7117b_6 - 0.4559b_7 \qquad (14)$$

where: b_2, b_3, b_4, b_5, b_6, b_7 represents the reflectance of Landsat8/OLI images in bands 2, 3, 4, 5, 6, and 7, respectively; Wet represents the humidity component of Landsat8/OLI images.

Heat

This work used Landsat 8 surface temperature to invert the land surface temperature (LST) to indicate the hotness indicator. The dual-band feature of Landsat 8 thermal infrared data offers the possibility of using a split-window algorithm to invert the surface temperature. Therefore, single-channel surface temperature inversion methods are mainly used in surface temperature inversion work to estimate surface temperature. This article chose the single window algorithm (SMW) proposed by *Ermida et al. (2020)*. The SMW algorithm is based on an empirical relationship between TOA brightness temperatures in a single TIR channel and LST and utilizes simple linear regression. The model consists of a linearization of the radiative transfer equation that maintains an explicit dependence on surface emissivity, and it is calculated as Eq. (15).

$$LST = A_i \frac{T_b}{\varepsilon} + B_i \frac{1}{\varepsilon} + C_i \qquad (15)$$

where T_b is the TOA brightness temperature in the TIR channel, and ε is the surface emissivity for the same channel. The algorithm coefficients A_i; B_i; and C_i are determined from linear regressions of radiative transfer simulations performed for 10 classes of Total Column Water Vapor (TCWV) that values from NCEP/NCAR reanalysis data are available on GEE ($I = 1, …, 10$), ranging from 0 to 6 cm in steps of 0.6 cm, with values of TCWV above 6 cm being assigned to the last class.

(4) Dryness

The dryness index represents an indicator of land dryness, which also indicates the degree of soil dryness and the land is affected by weathering and sanding. The dryness index consists of the normalized building bare soil index (NDBSI) incorporating the bare soil index (SI) and the building index (IBI), and the burned areas are mainly affected by the SI, and most burned areas are far from the towns and not easily affected by the IBI. Rikimaru's model was used to calculate the following Eq. (16).

$$SI = \frac{(\rho_{swir1} + \rho_{red}) - (\rho_{blue} + \rho_{NIR})}{(\rho_{swir1} + \rho_{red}) + (\rho_{blue} + \rho_{NIR})} \qquad (16)$$

Table 4 Extraction results of burned areas and their accuracy.

Time of fire	Heavy fire				Mild fire				Total burned area	
	dNBR_threshold1	Burned area (hm²)	Accuracy	Kappa	dNBR_threshold2	Burned area (hm²)	Accuracy	kappa	Burned area (hm²)	Accuracy
March 30, 2019	0.3010	43.20	98.4%	0.87	0.0654	77.62	95.38%	0.74	120.82	97.74%
March 28, 2020	0.3789	9,574.57	91.89%	0.81	0.1211	9,680.25	86.75%	0.71	19,254.82	89.32%
April 5, 2021	0.4024	66.81	98.96%	0.84	0.1464	159.59	93.79%	0.69	226.40	96.37%

where, ρ_{blue}, ρ_{red}, ρ_{swir1}, ρ_{NIR} denotes the reflectance of the blue band, red band, near-infrared band, and short-wave infrared band1 corresponding to the OLI image, respectively.

The proposed ecological index should be able to appear both as a single indicator and to combine the information from the above four indicators. Therefore, we used principal component analysis (PCA) (*Gewers et al., 2021*), a multivariate statistical method, to construct the ecological index. It is a multi-dimensional data compression technique that can select a few critical variables by an orthogonal linear transformation. Its most significant advantage is that the weights of the integrated indicators are not determined artificially; instead, they are determined automatically and objectively according to the contribution of each indicator to each principal component, thus avoiding the bias of the results caused by the different weight settings from a person.

Since the four indices are not uniform, it is necessary to normalize the original values of the four indices to a range between [0, 1] to avoid the imbalance of each index weight in the principal component analysis, and the normalization formula is as Eq. (17):

$$BI = (I_i - I_{min})/(I_{max} - I_{min}) \tag{17}$$

where, BI is the normalized image element value of a factor, I_i is the image element value of a factor, I_{max} and I_{min} the maximum and minimum values of the factor, respectively, the normalized indexes have a scale between 0 and 1. The normalized metrics are combined into a new image, and a principal component analysis is performed on the new image to obtain the first principal component (PC1) and related statistics. The obtained PCl is normalized to obtain the RSEI.

RESULTS

The extraction results of burned areas

According to the OTSU calculation, the heavily burned threshold and mildly burned threshold for each fire was obtained and then can get the heavily burned areas and mildly burned areas, and the two areas were added to get the total burned area. The results are shown in the following Table 4.
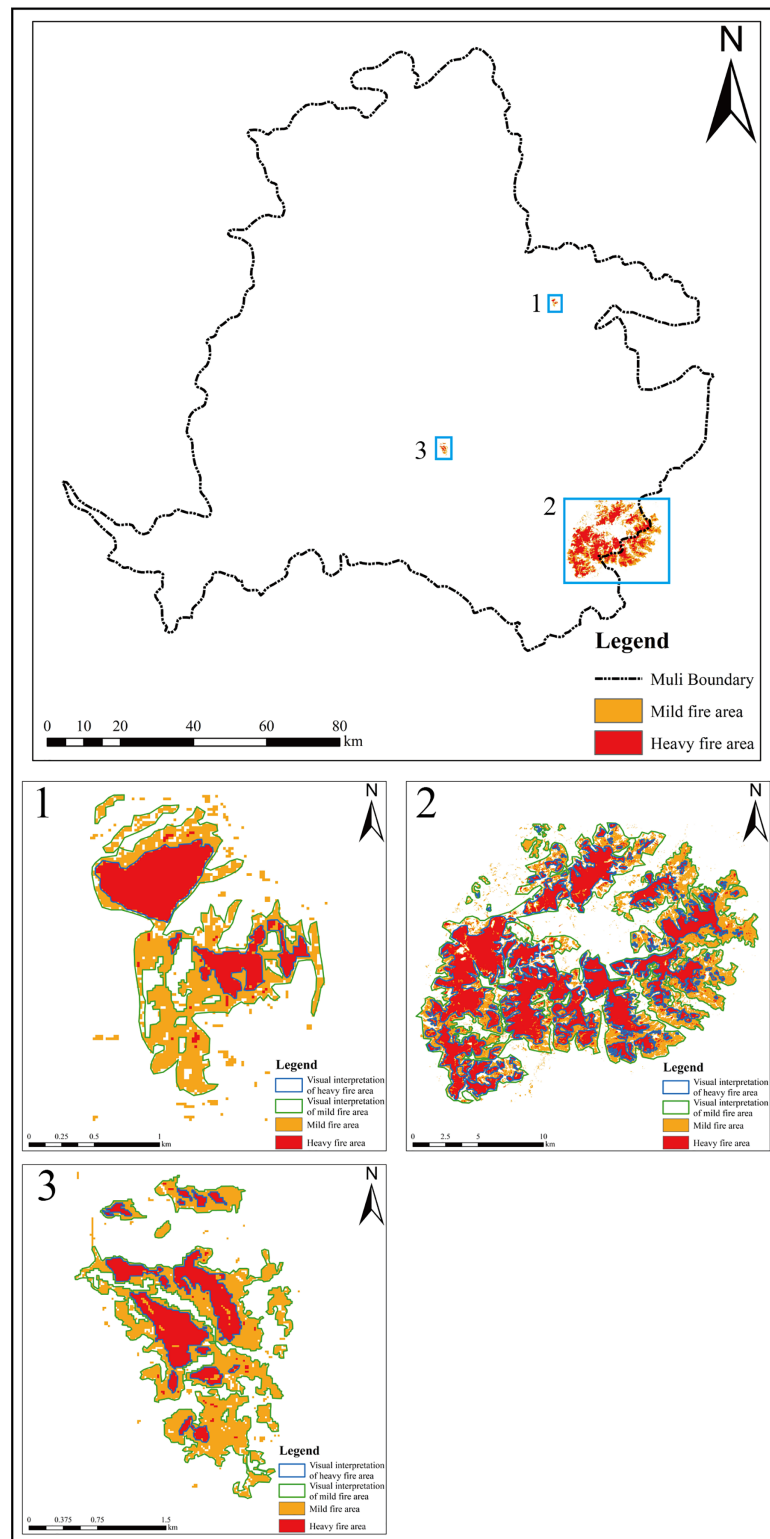
Figure 4 The burned area extraction map.

Table 5 The results of PCA.

		PC1	PC2	PC3	PC4
2019	Wet	0.6099	0.4007	0.3483	0.5884
	NDVI	0.5874	0.3296	0.2112	0.7083
	LST	−0.4084	−0.4847	−0.7028	−0.3228
	SI	−0.3409	−0.7042	−0.5831	−0.2189
	%	94.62	3.81	1.22	0.35
2020	Wet	0.6809	0.5059	0.3991	0.3480
	NDVI	0.4609	0.2654	0.6608	0.5296
	LST	−0.3879	−0.5829	−0.4239	−0.5745
	SI	−0.4165	−0.5778	−0.4735	−0.5181
	%	93.9	4.71	1.01	0.39
2021	Wet	0.6692	0.3997	0.6130	0.1289
	NDVI	0.4924	0.2753	0.5972	0.5702
	LST	−0.4878	−0.3993	−0.4107	−0.6587
	SI	−0.2677	−0.7778	−0.3145	−0.4737
	%	97.64	1.54	0.61	0.21

From Table 4, we can see that the accuracy of burned area extracted by combining the dNBR and OTSU thresholding image segmentation method for three fires was 97.69%, 89.32%, and 96.37%, respectively. The method performs better in the accuracy of small burned areas, but the performance is average in the extraction of the large burned area; the accuracy of heavily burned area extraction is higher than that of mildly burned.

Combined with the actual visual interpretation areas, the burned areas map derived from GEE using the OTSU threshold image segmentation method was compared, as shown in Fig. 4.

As can be seen, the heavily burned areas that were extracted matched the visual interpretation area, and the proposed method's accuracy is 98.4%, 91.89% and 98.96%, respectively. In contrast, the mildly burned areas are mainly distributed near the heavily burned areas, and the extracted burned areas are complete with clear boundaries and close to the visual interpretation results. However, it is difficult to intuitively extract the mildly burned areas and discriminate them from the remote sensing images.

Ecological environment evaluation results

As can be seen from Table 5, NDVI and wetness both played a positive role in promoting the ecological environment of the study area during the period, while SI and LST played a negative role together, which is consistent with the actual situation. The PC1's contribution in the calculation of the RSEI was more outstanding than 90%, indicating that the PC1 had concentrated most of the four indicators' information in the three fires; meanwhile, the four component indicators' contribution to PC1 was relatively stable, so PC1 was chosen to create the RSEI instead of the four component indicators.

Table 6 RSEI's mean values.

RSEI$_{mean}$	2019		2020		2021	
	Heavy fire area	Mild fire area	Heavy fire area	Mild fire area	Heavy fire area	Mild fire area
Pre-RSEI	0.6623	0.6674	0.6953	0.6971	0.7270	0.7484
Post-RSEI	0.4928	0.6036	0.5321	0.5910	0.4239	0.5894
Difference	0.1695	0.0638	0.1632	0.1061	0.3031	0.4106
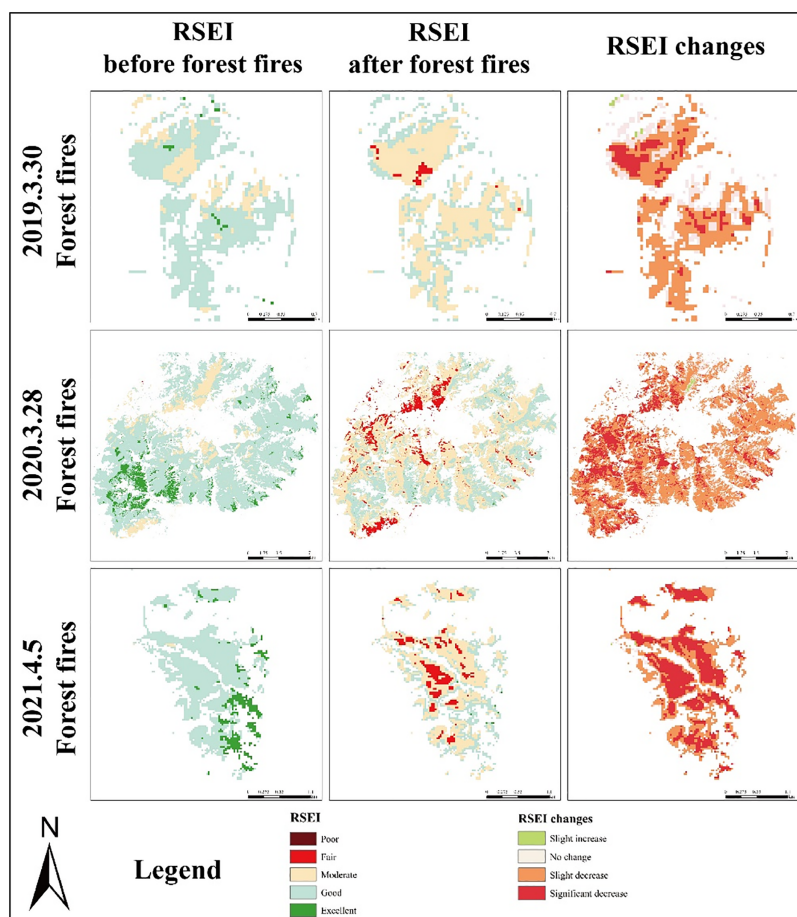
Figure 5 RSEI changes map.

The RESI's mean values were calculated from the results of PCA in before and after the fire as shown in the following Table 6.

We have concluded that the RSEI decreases significantly after three fires. To finely analyze the changes of RSEI, we calculated the difference of RESI before and after the fire for each pixel. Where −0.2 to −0.05 is a slight increase, −0.05 to 0.05 is no significant change, 0.05–0.20 is a slight decrease, and greater than 0.20 is a significant decrease. As shown in Fig. 5 below:

Table 7 RSEI's transfer matrix for heavily burned (a) and mildly burned (b) in 2019.

		Fire_pre					
		Poor	Fair	Moderate	Good	Excellent	Total
(a)							
Fire_post	Poor	0	0	0	0	0	0
	Fair	0	0	0.09	0	0	0.09
	Moderate	0	0	8.02	34.26	0	42.28
	Good	0	0	0	34.53	0.72	35.25
	Excellent	0	0	0	0	0	0
	Total	0	0	8.11	68.79	0.72	
	Change	0	0	0.09	34.26	0.72	
(b)							
Fire_post	Poor	0	0	0	0	0	0
	Fair	0	0	1.51	1.08	0	2.59
	Moderate	0	0	7.81	30.12	0.99	38.92
	Good	0	0	0	1.6	0.09	1.69
	Excellent	0	0	0	0	0	0
	Total	0	0	9.32	32.8	1.08	
	Change	0	0	1.51	31.2	1.08	

As we can see the Fig. 5, the following phenomena were present in all three fires: The post-RSEI of mildly burned and heavily burned was significantly lower than that of pre-RSEI, indicating that the fires brought different degrees of damage to the ecological environment; meanwhile, the difference in RSEI of heavy burned was higher than that of mildly burned, indicating that the damage of RSEI in the area of heavy burned was more serious, and the vegetation restoration measures in the area should be considered to reduce the impact of burned on the ecological environment as early as possible.

The monitoring analysis of the ecological environment

To further investigate the changes in the local ecological conditions, the normalized RSEI ecological index was divided into five levels according to the 0.2 value interval, from low to high: excellent: 0.8–1.0; good: 0.6–0.8; moderate: 0.4–0.6; fair: 0.2–0.4; poor: 0–0.2. We calculated the area and proportion of ecological classes before and after the three fires. And the transfer matrix was used to analyze the ecological changes as follows.

In 2019, we can see (Table 7) that the ecological environment of the burned areas changed: after the burn, the ecological environment had no excellent, but the poor ecological environment had an area of 0.09 hm^2; In the mildly burned area, the ecological environment changed from good to medium with an area of 34.26 hm^2, the changing area accounted for 49.8%, and all the excellent ecological environment changed to good. The ecological environment of the heavily burned area had changed more, and it has a poor with an area of 2.59 hm^2, the excellent ecological environment (1.08 hm^2) changed to

Table 8 RSEI's transfer matrix for heavily burned (a) and mildly burned (b) in 2020.

		Fire_pre					
		Poor	Fair	Moderate	Good	Excellent	Total
(a)							
Fire_post	Poor	0	0.54	2.88	0.72	0.09	4.23
	Fair	0	0.72	310.08	122.67	3.06	436.53
	Moderate	0	0	513.99	3,962.3	70.74	4,547.03
	Good	0	0	0	4,130.75	512.75	4,643.5
	Excellent	0	0	0	0	48.96	48.96
	Total	0	1.26	826.95	8,216.44	635.6	
	Change	0	0.54	312.96	4,085.69	586.64	
(b)							
Fire_post	Poor	0	0	4.45	5.11	0.09	9.65
	Fair	0	0.09	539.52	516.75	7.55	1,063.91
	Moderate	0	0	476.81	5,178.1	202.12	5,857.03
	Good	0	0	0	2,118.84	517.04	2,635.88
	Excellent	0	0	0	0	8.1	8.1
	Total	0	0.09	1,020.78	7,818.8	734.9	
	Change	0	0	543.97	5,699.96	726.8	

a medium (0.99 hm^2) ecological environment with accounted for 95.12%, which means that the ecological environment of the heavily burned area has changed more prominently.

In 2020, there was no poor ecological environment before the fire (Table 8), but poor ecological conditions appeared after the fire with an area of 13.88 hm^2. The areas of the excellent ecological environment also decreased from 1,370.5 to 57.06 hm^2. In the mildly burned areas, the ecological environment was concentrated in the good ecological environment before the fire, but after the fire, its ecological environment changed to medium grade, accounting for 49.73% (3,962.3 hm^2), and the ecological environment changed from excellent to good grade, and it accounted for 92.30%. In the heavily burned area, the ecological environment evaluation was concentrated in the good grade, but it was concentrated in the medium grade after the fire. Changes in the ecological environment were concentrated in the pre-fire good and excellent ecological environment, and most of the excellent ecological environment was changed to the medium or poor ecological environment, with accounted for 98.90%, and most of the good ecological environment was changed to the medium ecological environment with accounted for 72.90%.

Also, we can see (Table 9) that the ecological environment of the burned area changed in 2021: before the fire, there was no poor ecological environment, but after the fire, there was a poor ecological environment with an area of 27.38 hm^2, while the excellent ecological environment changed from 32.68 to 0.63 hm^2 with accounted for 61.51%, and the excellent ecological environment changed to good or medium with accounted for 97.93%; In the heavily burned area: medium ecological environment all changed to the worse ecological environment with accounted for 100%, and good ecological environment changed to the

Table 9 RSEI's transfer matrix for heavily burned (a) and mildly burned (b) in 2021.

		Fire_pre					
		Poor	Fair	Moderate	Good	Excellent	Total
(a)							
Fire_post	Poor	0	0	0	0	0	0
	Fair	0	0	0.09	25.85	0.09	26.03
	Moderate	0	0	0	38.01	1.51	39.52
	Good	0	0	0	0.63	0.63	1.26
	Excellent	0	0	0	0	0	0
	Total	0	0	0.09	64.49	2.23	
	Change	0	0	0.09	63.86	2.23	
(b)							
Fire_post	Poor	0	0	0	0	0	0
	Fair	0	0	0.09	1.26	0	1.35
	Moderate	0	0	0.9	78.83	10.7	90.43
	Good	0	0	0	48.06	19.12	67.18
	Excellent	0	0	0	0	0.63	0.63
	Total	0	0	0.99	128.15	30.45	
	Change	0	0	0.09	80.09	29.82	

worse or medium ecological environment with accounted for 99.02%, excellent ecological environment mainly changed to the medium and worse ecological environment with accounted for 100%.

In summary, there was no poor ecological environment in the three pre-fires, but the ecology showed a poor level after being burned in high fire intensity in 2020 and no poor level after the 2019 and 2021 fires. So in terms of area burned and ecological changes, the fires in 2020 were more severe than those in 2019 and 2020. On the other hand, regardless of the heavily burned area and mildly burned area, the pre-fire ecology had a good area, but its post-fire ecology change area was also the largest, and the post-fire ecology had the most moderate area. It shows that the ecological environment changed from good to moderate after the fire.

DISCUSSION

Forest fires are frequent and costly, so it is crucial to use remote sensing techniques to quickly extract burned areas and assess their ecological change (*Liu, Ballantyne & Cooper, 2019*; *Mota et al., 2019*). Remote sensing images have the advantages of low cost, high accuracy, and high efficiency, and they play an essential role in fire scene identification and burning.

Remote sensing burn indices are often used for extracting burned areas, but most of the studies have focused on major fires (burned area over 100 km^2) (*Tian et al., 2022*), and the applicability of the method has rarely been evaluated. On the other hand, the often used remote sensing data, such as sentinel-2, Gaofen, *etc.*, have a high spatial resolution, large

storage space and low data processing efficiency, which means that their wide industrial application may be limited. In order to get accurate information and dynamics of forest fires, efficient and reliable forest fire identification algorithms are especially important. In this study, using sentinel-2 remote sensing data on the GEE platform, we used the idea of a decision tree to extract the burning area of three fires in Muli County by combining the dNBR and OTSU thresholding methods. Accuracy comparing the results of the method using the remote sensing technology with the published research results.

Among them, in 2019, compared with *Rao, Wang & Huang (2020)*, the accuracy of heavy burning was improved by 3.73%, the accuracy of light burning was improved by 4.44%, and the overall accuracy was improved by 7.03%. In 2020, *Li et al. (2021a)* extracted a burned area of 180.37 km^2 by calculating the Difference Normalized Vegetation Index (dNDVI) from Landsat 8 remote sensing imagery km. However, the area visually interpreted in that study was 204.54 km^2, while the area extracted in this study was 192.55 km^2, while *Tian et al. (2022)*, based on the visual interpretation results of Li et al. extracted the burning area of 209.17 km^2 using Sentinel-2 images combined with dNBR, which improved the accuracy compared with the area of 204.54 km^2 based on the visual interpretation of Landsat 8 remote sensing images. However, the empirical threshold method was used in that study. In this study, the burned area extracted by using the OTSU automatic extraction threshold method in this study is 192.55 km^2, which is close to the fire survey data of the Sichuan Forestry Survey and Design Institute obtained visual interpretation based on Sentinel-2 remote sensing images. No study has been published for the 2021 Muli fire, and the area burned in Muli County in 2021 has not been monitored in the remote sensing fire product MOD14A2 resolution due to its large spatial resolution (1 km). Therefore, this method can extract the burning area of smaller fires more accurately, but the extraction accuracy is lower for larger fires such as the 2019 fire, which may be potentially due to fire having heterogeneous effects at scales finer than 30 m, particularly in non-stand replacing fires, resulting in high sub-pixel variability in tree mortality (*Schroeter & Foster, 2004*; *Howe et al., 2022*) and frequency of smaller-sized unburned patches. However, the larger the area, the greater the heterogeneity of fire images presented, so it is also a question of whether to choose a more accurate way, such as deep learning, to extract the burning area in the method for a higher spatial resolution.
In addition, the accuracy of this method for extracting heavily burned area is higher than that of mildly burned area, which is similar to the study of *Zhang et al. (2021)* and *Silva-Cardoza et al. (2022)*, In addition, the novelty of this method lies in the rapid acquisition of before and after fire images through the GEE cloud computing platform. GEE and the developed algorithm are very attractive and suitable for providing near real-time burned area maps in that both burned areas and the different levels of burn severity can be identified automatically and without using fixed threshold values. So the method proposed in this article can quickly and accurately extract the burned area and provide important information for the subsequent assessment of ecological changes before and after the fire.

The changes in vegetation cover before and after the fire have been studied (*Zhou et al., 2019*), but fire also brings changes to the ecological environment, such as soil moisture and heat. So the ecological changes of different degrees of fire also provide basic information
for the subsequent environmental restoration. In this article, the ecological environment changes before and after the fires were evaluated using the RSEI remote sensing ecological index, and it is obvious to see in the three fires that the ecological environment changes more in the heavy fires, so whether to intervene artificially in the ecological environment restoration of the heavily burned area is also one of the future research priorities.

In addition, the natural conditions of the study area do create prerequisites for fires to occur, as it is located in the Hengduan Mountains, with complex topography, high mountains and dense forests. Most areas are primitive forests with dense vegetation, where Yunnan pine and other species commonly grow and are rich in oil. Together with the long-term accumulation of dead branches and leaves forming the ground humus layer, all provide combustible material conditions for forest fires to break out. In addition, the mountain landscape is complex, and the terrain is highly undulating; fire spread was accelerated because of the steep mountain environment. The region should focus on highlighting the mechanized forest firefighting professional team equipment construction to improve the ability to deal with forest fires.

Furthermore, what measures should be taken to restore the vegetation in the burned area? It should be considered the fire intensity, fire area and the natural renewal characteristics of the original vegetation in the area. With time, the mildly burned areas will naturally recover to the pre-fire state, and no excessive artificial disturbance measures are usually needed. For heavily burned areas, if the soil conditions are good, can be considered for vegetation restoration measures to speed up forest restoration and achieve economic benefits as early as possible, such as artificial or semi-artificial disturbances. So which stage of fire area restoration to take disturbance measures and what disturbance measures to take are essential elements of scientific research; if the stand conditions of burned areas are poor, such as high mountains and steep slopes, infertile soil, *etc.*, such as March 30, 2019, Sichuan Muli County heavy burned area, it is not suitable to take more artificial disturbance measures except for the necessary aircraft seeding to provide seed source.

CONCLUSIONS

Muli County is a national fire risk area. This study clarified the burned area caused by three fires based on the dNBR index calculated from sentinel-2 remote sensing images, while combining the OTSU threshold and the decision tree methods. On March 30, 2019, the burned area was 120.82 hm^2, of which the heavily burned area (forest loss area) was 43.20 hm^2 and the mildly burned area (fire traced area) was 77.62 hm^2; on March 28, 2020, the burned area was 19,254.82 hm^2, of which 9,574.57 hm^2 is heavily burned area (forest loss area), and 9,680.25 hm^2 is mildly burned areas (fire traced area), March 30, 2019, burned area is 226.40 hm^2, of which 66.81 hm^2 is heavily burned area (forest loss area) and 159.59 hm^2 is mildly burned areas (fire traced area). The accuracy verification with the visual interpretation results obtained 97.69%, 89.32%, and 96.37% extraction accuracy based on field survey data. This result improved our understanding of the ecological quality changes through a forest fire and helped the post-fire vegetation recovery.

Meanwhile, the RSEI remote sensing index was used to quantitatively evaluate the ecological environment changes in the three fires. It concluded that RSEI after the three forest fires was significantly lower than that before the fires, indicating that the fires brought different degrees of damage to the ecological environment in the area. Also, the RSEI difference of the heavily burned area fires was higher than that of the mildly burned areas; from the two dimensions of heavily burned areas and mildly burned areas, the area changes of forest RSEI before and after the three fires were quantified by using the transfer matrix. It is quantitatively analyzed the damage caused by fire to the ecosystem.

Funding

This research was supported by the Second National Survey of Key Protected Wild Plant Resources-Special Survey of Orchidaceae in Sichuan Province (No. 80303-AZZ003), the Special Project of Orchid Survey of National Forestry and Grassland Administration (No. 2019073015) and the Second Tibetan Plateau Scientific Expedition and Research Program (STEP), China (No. 2019QZKK0301). The funders had no role in study design, data collection and analysis, decision to publish, or preparation of the manuscript.

Grant Disclosures

The following grant information was disclosed by the authors:
National Survey of Key Protected Wild Plant Resources-Special Survey of Orchidaceae in Sichuan Province: 80303-AZZ003.
Orchid Survey of National Forestry and Grassland Administration: 2019073015.
Second Tibetan Plateau Scientific Expedition and Research Program (STEP), China: 2019QZKK0301.

Competing Interests

The authors declare that they have no competing interests.

Author Contributions

- Shiqi Zhang conceived and designed the experiments, performed the experiments, analyzed the data, prepared figures and/or tables, authored or reviewed drafts of the article, and approved the final draft.
- Maoyang Bai conceived and designed the experiments, performed the experiments, analyzed the data, prepared figures and/or tables, authored or reviewed drafts of the article, and approved the final draft.
- Xiao Wang analyzed the data, authored or reviewed drafts of the article, and approved the final draft.
- Xuefeng Peng analyzed the data, authored or reviewed drafts of the article, and approved the final draft.
- Ailin Chen performed the experiments, authored or reviewed drafts of the article, and approved the final draft.

- Peihao Peng conceived and designed the experiments, authored or reviewed drafts of the article, and approved the final draft.

Data Availability

The raw data and code are available in the Supplemental Files.

Supplemental Information

Supplemental information for this article can be found online at http://dx.doi.org/10.7717/peerj.14557#supplemental-information.

REFERENCES

Andela N, Morton DC, Giglio L, Chen Y, Van Der Werf GR, Kasibhatla PS, DeFries RS, Collatz GJ, Hantson S, Kloster S, Bachelet D, Forrest M, Lasslop G, Li F, Mangeon S, Melton JR, Yue C, Randerson JT. 2017. A human-driven decline in global burned area. *Science* **356(6345)**:1356–1362 DOI 10.1126/science.aal4108.

Attorre F, Govender N, Hausmann A, Farcomeni A, Guillet A, Scepi E, Smit IPJ, Vitale M. 2015. Assessing the effect of management changes and environmental features on the spatio-temporal pattern of fire in an African Savanna. Fire spatio-temporal pattern. *Journal for Nature Conservation* **28(1)**:1–10 DOI 10.1016/j.jnc.2015.07.001.

Ba R, Song W, Li X, Xie Z, Lo S. 2019. Integration of multiple spectral indices and a neural network for burned area mapping based on MODIS data. *Remote Sensing* **11(3)**:326 DOI 10.3390/rs11030326.

Baig MHA, Zhang L, Shuai T, Tong Q. 2014. Derivation of a tasselled cap transformation based on Landsat 8 at-satellite reflectance. *Remote Sensing Letters* **5(5)**:423–431 DOI 10.1080/2150704X.2014.915434.

Chen D, Loboda TV, Hall JV. 2020. A systematic evaluation of influence of image selection process on remote sensing-based burn severity indices in North American boreal forest and tundra ecosystems. *ISPRS Journal of Photogrammetry and Remote Sensing* **159**:63–77 DOI 10.1016/j.isprsjprs.2019.11.011.

Chia EK, Bassett M, Leonard SWJ, Holland GJ, Ritchie EG, Clarke MF, Bennett AF. 2016. Effects of the fire regime on mammal occurrence after wildfire: site effects vs landscape context in fire-prone forests. *Forest Ecology and Management* **363(10)**:130–139 DOI 10.1016/j.foreco.2015.12.008.

Chuvieco E, Aguado I, Salas J, García M, Yebra M, Oliva P. 2020. Satellite remote sensing contributions to wildland fire science and management. *Current Forestry Reports* **6(2)**:81–96 DOI 10.1007/s40725-020-00116-5.

Chuvieco E, Martín MP, Palacios A. 2010. Assessment of different spectral indices in the red-near-infrared spectral domain for burned land discrimination. *International Journal of Remote Sensing* **23(23)**:5103–5110 DOI 10.1080/01431160210153129.

Cocke AE, Fulé PZ, Crouse JE. 2005. Comparison of burn severity assessments using Differenced Normalized Burn Ratio and ground data. *International Journal of Wildland Fire* **14(2)**:189–198 DOI 10.1071/WF04010.

Day NJ, White AL, Johnstone JF, Degré-timmons GÉ, Cumming SG, Mack MC, Turetsky MR, Walker XJ, Baltzer JL. 2020. Fire characteristics and environmental conditions shape plant communities via regeneration strategy. *Ecography* **43(10)**:1464–1474 DOI 10.1111/ecog.05211.

De Faria BL, Brando PM, Macedo MN, Panday PK, Soares-Filho BS, Coe MT. 2017. Current and future patterns of fire-induced forest degradation in Amazonia. *Environmental Research Letters* **12(9)**:95005 DOI 10.1088/1748-9326/aa69ce.

Dutta K, Talukdar D, Bora SS. 2022. Segmentation of unhealthy leaves in cruciferous crops for early disease detection using vegetative indices and Otsu thresholding of aerial images. *Measurement: Journal of the International Measurement Confederation* **189**:110478 DOI 10.1016/j.measurement.2021.110478.

Epting J, Verbyla D, Sorbel B. 2005. Evaluation of remotely sensed indices for assessing burn severity in interior Alaska using Landsat TM and ETM+. *Remote Sensing of Environment* **96(3–4)**:328–339 DOI 10.1016/j.rse.2005.03.002.

Ermida SL, Soares P, Mantas V, Göttsche FM, Trigo IF. 2020. Google earth engine open-source code for land surface temperature estimation from the landsat series. *Remote Sensing* **12(9)**:1–21 DOI 10.3390/rs12091471.

Fan C-D, Ren K, Zhang Y-J, Yi L-Z. 2016. Optimal multilevel thresholding based on molecular kinetic theory optimization algorithm and line intercept histogram. *Journal of Central South University* **23(4)**:880–890 DOI 10.1007/s11771-016-3135-8.

Forkel M, Dorigo W, Lasslop G, Chuvieco E, Hantson S, Heil A, Teubner I, Thonicke K, Harrison SP. 2019. Recent global and regional trends in burned area and their compensating environmental controls. *Environmental Research Communications* **1(5)**:51005 DOI 10.1088/2515-7620/ab25d2.

Franquesa M, Lizundia-Loiola J, Stehman SV, Chuvieco E. 2022. Using long temporal reference units to assess the spatial accuracy of global satellite-derived burned area products. *Remote Sensing of Environment* **269(4)**:112823 DOI 10.1016/j.rse.2021.112823.

Gao Y, Skutsch M, Paneque-Gálvez J, Ghilardi A. 2020. Remote sensing of forest degradation: a review. *Environmental Research Letters* **15(10)**:103001 DOI 10.1088/1748-9326/abaad7.

Gewers FL, Ferreira GR, De Arruda HF, Silva FN, Comin CH, Amancio DR, Costa LDF. 2021. Principal component analysis: a natural approach to data exploration. *ACM Computing Surveys* **54(4)**:1–33 DOI 10.1145/3447755.

Ghatkar JG, Singh RK, Shanmugam P. 2019. Classification of algal bloom species from remote sensing data using an extreme gradient boosted decision tree model. *International Journal of Remote Sensing* **40(24)**:9412–9438 DOI 10.1080/01431161.2019.1633696.

Giri S, Qiu Z, Zhang Z. 2017. A novel technique for establishing soil topographic index thresholds in defining hydrologically sensitive areas in landscapes. *Journal of Environmental Management* **200(8)**:391–399 DOI 10.1016/j.jenvman.2017.04.080.

Gitas I, Mitri G, Veraverbeke S, Polychronaki A. 2012. Advances in remote sensing of post-fire vegetation recovery monitoring—A review. In: *Remote Sensing of Biomass—Principles and Applications.* Norderstedt: Books on Demand.

Hall JV, Loboda TV, Giglio L, McCarty GW. 2016. A MODIS-based burned area assessment for Russian croplands: mapping requirements and challenges. *Remote Sensing of Environment* **184(1)**:506–521 DOI 10.1016/j.rse.2016.07.022.

Howe AA, Parks SA, Harvey BJ, Saberi SJ, Lutz JA, Yocom LL. 2022. Comparing Sentinel-2 and Landsat 8 for burn severity mapping in Western North America. *Remote Sensing* **14(20)**:1–21 DOI 10.3390/rs14205249.

Huang M, Jin S. 2020. Rapid flood mapping and evaluation with a supervised classifier and change detection in Shouguang using Sentinel-1 SAR and Sentinel-2 optical data. *Remote Sensing* **12(13)**:2073 DOI 10.3390/rs12132073.

Jiang F, Zhang Y, Li J, Sun Z. 2021. Research on remote sensing ecological environmental assessment method optimized by regional scale. *Environmental Science and Pollution Research* **28(48)**:68174–68187 DOI 10.1007/s11356-021-15262-x.

Kim T, Hwang S, Choi J. 2021. Characteristics of spatiotemporal changes in the occurrence of forest fires. *Remote Sensing* **13(23)**:4940 DOI 10.3390/rs13234940.

Laneve G, Fusilli L, Bernini G, Beltran JS. 2020. Preventing forest fires through remote sensing. *IEEE Geoscience and Remote Sesing Magazine* **20**:2–14 DOI 10.1109/MGRS.2019.2906948.

Li Q, Cui J, Jiang W, Jiao Q, Gong L, Zhang J, Shen X. 2021a. Monitoring of the Fire in Muli County on March 28, 2020, based on high temporal-spatial resolution remote sensing techniques. *Natural Hazards Research* **1(1)**:20–31 DOI 10.1016/j.nhres.2021.02.001.

Li B, Zhou J, Bu J, Qin X, Cheng X, Pan B, Feng J. 2021b. Analysis of forest fire causes and application of lightning monitoring data in Muli County. *Journal of Catastrophology* **36**:125–132 DOI 10.3969/j.issn.1000-811X.2021.03.022.

Li W, Zhu J, Fu L, Zhu Q, Guo Y, Gong Y. 2021c. A rapid 3D reproduction system of dam-break floods constrained by post-disaster information. *Environmental Modelling and Software* **139(2)**:104994 DOI 10.1016/j.envsoft.2021.104994.

Li W, Zhu J, Fu L, Zhu Q, Xie Y, Hu Y. 2021d. An augmented representation method of debris flow scenes to improve public perception. *International Journal of Geographical Information Science* **35(8)**:1521–1544 DOI 10.1080/13658816.2020.1833016.

Lian Z, Hao H, Zhao J, Cao K, Wang H, He Z. 2022. Evaluation of remote sensing ecological index based on soil and water conservation on the effectiveness of management of abandoned mine landscaping transformation. *International Journal of Environmental Research and Public Health* **19(15)**:1–15 DOI 10.3390/ijerph19159750.

Liu H. 2014. Analysis of forest fire prevention in forest areas of Muli County. *Journal of Green Science and Technology* **9**:234–237 DOI 10.3969/j.issn.1674-9944.2014.09.104.

Liu Z, Ballantyne AP, Cooper LA. 2019. Biophysical feedback of global forest fires on surface temperature. *Nature Communications* **10(1)**:1–9 DOI 10.1038/s41467-018-08237-z.

Mallinis G, Mitsopoulos I, Chrysafi I. 2018. Evaluating and comparing sentinel 2A and landsat-8 operational land imager (OLI) spectral indices for estimating fire severity in a mediterranean pine ecosystem of Greece. *GIScience and Remote Sensing* **55(1)**:1–18 DOI 10.1080/15481603.2017.1354803.

Mitchard ETA. 2018. The tropical forest carbon cycle and climate change. *Nature* **559(7715)**:527–534 DOI 10.1038/s41586-018-0300-2.

Mitri GH, Gitas IZ. 2008. Mapping the severity of fire using object-based classification of IKONOS imagery. *International Journal of Wildland Fire* **17(3)**:431–442 DOI 10.1071/WF07103.

Mota PHS, da Rocha SJSS, de Castro NLM, Marcatti GE, de França LCJ, Schettini BLS, Villanova PH, dos Santos HT, dos Santos AR. 2019. Forest fire hazard zoning in Mato Grosso State. *Brazil Land Use Policy* **88(1)**:104206 DOI 10.1016/j.landusepol.2019.104206.

Mueller EV, Skowronski N, Clark K, Gallagher M, Kremens R, Thomas JC, El Houssami M, Filkov A, Hadden RM, Mell W, Simeoni A. 2017. Utilization of remote sensing techniques for the quantification of fire behavior in two pine stands. *Fire Safety Journal* **91**:845–854 DOI 10.1016/j.firesaf.2017.03.076.

Otsu N. 1979. A threshold selection method from gray-level histograms. *IEEE Transactions on Systems, Man, and Cybernetics* **9(1)**:62–66 DOI 10.1109/TSMC.1979.4310076.

Otsu N. 1996. A threshold selection method from gray-level histograms. *IEEE Transactions on Systems, Man, and Cybernetics* **9(1)**:62–66 DOI 10.1109/TSMC.1979.4310076.

Pan F, Xi X, Wang C. 2020. A comparative study of water indices and image classification algorithms for mapping inland surface water bodies using landsat imagery. *Remote Sensing* **12(10)**:1611 DOI 10.3390/rs12101611.

Pezzatti GB, De Angelis A, Bekar İ, Ricotta C, Bajocco S, Conedera M. 2020. Complementing daily fire-danger assessment using a novel metric based on burnt area ranking. *Agricultural and Forest Meteorology* **295(2)**:1–10 DOI 10.1016/j.agrformet.2020.108172.

Rao Y, Wang C, Huang H. 2020. Forest fire monitoring based on multisensor remote sensing techniques in Muli County. *Journal of Remote Sensing* **25**:559–570 [in Chinese] DOI 10.11834/jrs.20209125.

Reddy CS, Bird NG, Sreelakshmi S, Manikandan TM, Asra M, Krishna PH, Jha CS, Rao PVN, Diwakar PG. 2019. Identification and characterization of spatio-temporal hotspots of forest fires in South Asia. *Environmental Monitoring and Assessment* **191(S3)**:46 DOI 10.1007/s10661-019-7695-6.

Roteta E, Bastarrika A, Franquesa M, Chuvieco E. 2021. Landsat and sentinel-2 based burned area mapping tools in google earth engine. *Remote Sensing* **13(4)**:1–30 DOI 10.3390/rs13040816.

Santana NC, de Carvalho Júnior OA, Gomes RAT, Guimarães RF. 2020. Accuracy and spatiotemporal distribution of fire in the Brazilian biomes from the MODIS burned-area products. *International Journal of Wildland Fire* **29(10)**:907–918 DOI 10.1071/WF19044.

Schroeter C, Foster K. 2004. The impact of health information and demographic changes on aggregate meat demand. ENEPRI Policy Brief No. 4:476–486. *Available at https://EconPapers. repec.org/RePEc:ags:aaea04:20130*.

Sekertekin A. 2021. A survey on global thresholding methods for mapping open water body using Sentinel-2 satellite imagery and normalized difference water index. *Archives of Computational Methods in Engineering* **28(3)**:1335–1347 DOI 10.1007/s11831-020-09416-2.

Seydi ST, Akhoondzadeh M, Amani M, Mahdavi S. 2021. Wildfire damage assessment over Australia using Sentinel-2 imagery and MODIS land cover product within the google earth engine cloud platform. *Remote Sensing* **13(2)**:1–30 DOI 10.3390/rs13020220.

Silva-Cardoza AI, Vega-Nieva DJ, Briseño-Reyes J, Briones-Herrera CI, López-Serrano PM, Corral-Rivas JJ, Parks SA, Holsinger LM. 2022. Evaluating a new relative phenological correction and the effect of sentinel-based earth engine compositing approaches to map fire severity and burned area. *Remote Sensing* **14(13)**:3122 DOI 10.3390/rs14133122.

Smith AMS, Drake NA, Wooster MJ, Hudak AT, Holden ZA. 2007. Production of Landsat ETM+ reference imagery of burned areas within Southern African savannahs: comparison of methods and application to MODIS. *International Journal of Remote Sensing* **28(12)**:2753–2775 DOI 10.1080/01431160600954704.

Sudhakar S, Vijayakumar V, Sathiya Kumar C, Priya V, Ravi L, Subramaniyaswamy V. 2020. Unmanned aerial vehicle (UAV) based forest fire detection and monitoring for reducing false alarms in forest-fires. *Computer Communications* **149(7)**:1–16 DOI 10.1016/j.comcom.2019.10.007.

Sun G, Qin X, Liu S, Li X, Chen X, Zhong X. 2019. Potential analysis of typical vegetation index for identifying burned area. *Remote Sensing for Land and Resources* **31**:204–211 DOI 10.6046/gtzyyg.2019.01.27.

Sun Q, Wu Z, Tan J. 2012. The relationship between land surface temperature and land use/land cover in Guangzhou, China. *Environmental Earth Sciences* **65(6)**:1687–1694 DOI 10.1007/s12665-011-1145-2.

Tang R, Wang L, Zhao J, Wang A. 2021. Monitoring "3·28" forest fire emergency disaster in Sichuan Muli based on remote sensing technology. *Land and Resources Informatization* **1**:12–18 DOI 10.3969/j.issn.1674-3695.2021.01.003.

Tian Y, Wu Z, Li M, Wang B, Zhang X. 2022. Forest fire spread monitoring and vegetation dynamics detection based on multi-source remote sensing images. *Remote Sensing* **14(18)**:1–20 DOI 10.3390/rs14184431.

Tianchi L, Fuqin Y, Yan L. 2020. Forest fire monitoring based on Sentinel-2 image in Muli, Sichuan Province. *South China Forestry Science* **48**:49–53 DOI 10.16259/j.cnki.36-1342/s.2020.06.011.

Valencia GM, Anaya JA, Velásquez ÉA, Ramo R, Caro-Lopera FJ. 2020. About validation-comparison of burned area products. *Remote Sensing* **12(23)**:1–23 DOI 10.3390/rs12233972.

Vargas-Cuentas NI, Roman-Gonzalez A. 2021. Satellite-based analysis of forest fires in the Bolivian Chiquitania and Amazon Region: case 2019. *IEEE Aerospace and Electronic Systems Magazine* **36(2)**:38–54 DOI 10.1109/MAES.2020.3033392.

Verma AK, Garg PK, Hari Prasad KS. 2017. Sugarcane crop identification from LISS IV data using ISODATA, MLC, and indices based decision tree approach. *Arabian Journal of Geosciences* **10(1)**:27 DOI 10.1007/s12517-016-2815-x.

Wang J, Li G. 2022. Eco-environmental effect evaluation of *Tamarix chinesis* forest on coastal saline-alkali land based on RSEI model. *Sensors Article* **22(13)**:1–19 DOI 10.3390/s22135052.

Xaud HAM, da Martins FSRV, Dos Santos JR. 2013. Tropical forest degradation by mega-fires in the northern Brazilian Amazon. *Forest Ecology and Management* **294(L07701)**:97–106 DOI 10.1016/j.foreco.2012.11.036.

Xu H. 2013. A remote sensing index for assessment of regional ecological changes. *China Environmental Science* **33**:889–897 DOI 10.3969/j.issn.1000-6923.2013.05.019.

Yang CC, Prasher SO, Enright P, Madramootoo C, Burgess M, Goel PK, Callum I. 2003. Application of decision tree technology for image classification using remote sensing data. *Agricultural Systems* **76(3)**:1101–1117 DOI 10.1016/S0308-521X(02)00051-3.

Yuan B, Fu L, Zou Y, Zhang S, Chen X, Li F, Deng Z, Xie Y. 2021. Spatiotemporal change detection of ecological quality and the associated affecting factors in Dongting Lake Basin, based on RSEI. *Journal of Cleaner Production* **302(Suppl. 1)**:126995 DOI 10.1016/j.jclepro.2021.126995.

Zhang Y, Ling F, Wang X, Foody GM, Boyd DS, Li X, Du Y, Atkinson PM. 2021. Tracking small-scale tropical forest disturbances: fusing the Landsat and Sentinel-2 data record. *Remote Sensing of Environment* **261**:112470 DOI 10.1016/j.rse.2021.112470.

Zhang X, Treitz PM, Chen D, Quan C, Shi L, Li X. 2017. Mapping mangrove forests using multi-tidal remotely-sensed data and a decision-tree-based procedure. *International Journal of Applied Earth Observation and Geoinformation* **62(2)**:201–214 DOI 10.1016/j.jag.2017.06.010.

Zhang J, Zhang J, Dai T, He Z. 2019. Exploring weighted dual graph regularized non-negative matrix tri-factorization based collaborative filtering framework for multi-label annotation of remote sensing images. *Remote Sensing* **11(8)**:922 DOI 10.3390/rs11080922.

Zhao Z, Li W, Ciais P, Santoro M, Cartus O, Peng S, Yin Y, Yue C, Yang H, Yu L, Zhu L, Wang J. 2021a. Fire enhances forest degradation within forest edge zones in Africa. *Nature Geoscience* **14(7)**:479–483 DOI 10.1038/s41561-021-00763-8.

Zhao B, Zhuang Q, Shurpali N, Köster K, Berninger F, Pumpanen J. 2021b. North American boreal forests are a large carbon source due to wildfires from 1986 to 2016. *Scientific Reports* **11(1)**:1–14 DOI 10.1038/s41598-021-87343-3.

Zhou Z, Liu L, Jiang L, Feng W, Samsonov SV. 2019. Using long-term SAR backscatter data to monitor post-fire vegetation recovery in tundra environment. *Remote Sensing* **11(19)**:1–20 DOI 10.3390/rs11192230.

Zhou G, Zhang R, Zhang D. 2016. Manifold learning co-location decision tree for remotely sensed imagery classification. *Remote Sensing* **8(10)**:1–31 DOI 10.3390/rs8100855.